
Design and certification of a composite thin-walled structure for energy absorption

Paolo Feraboli*

Department of Aeronautics and Astronautics,
University of Washington,
Box 352400,
Seattle, WA 98195-2400, USA
E-mail: feraboli@aa.washington.edu
*Corresponding author

Chris Norris and Doug McLarty

Swift Engineering Inc.,
San Clemente, CA 92673, USA

Abstract: Thin-walled Carbon Fibre Reinforced Polymer (CFRP) energy-absorbing devices have been successfully used in premier racing leagues to drastically improve the crashworthiness of a vehicle. Since their introduction in Formula 1 (F1) in the second half of the 1990s, the Rear Impact (RIMP) attenuators have received particular attention and their utilisation has been documented in scholarly publications. The engineering development and certification of the RIMP of the Star Mazda Racecar is discussed in detail. Quasi-static and dynamic crush tests are performed on two RIMP designs, featuring very different stacking sequences, are experimentally investigated. While the overall behaviour is quite different, they both exhibit the ability to collapse in a stable, progressive fashion. Furthermore, although the overall shape of the load-stroke diagram, energy absorption characteristics and failure behaviour have shown very good agreement, the quasi-static test results tend to substantially overestimate the effective dynamic energy absorption characteristics. The final RIMP design is selected based on its higher energy absorption and friendlier manufacturing characteristics.

Keywords: carbon fibre; composites; crashworthiness; energy absorption; impact; destructive testing; racecar.

Reference to this paper should be made as follows: Feraboli, P., Norris, C. and McLarty, D. (2007) 'Design and certification of a composite thin-walled structure for energy absorption', *Int. J. Vehicle Design*, Vol. 44, Nos. 3/4, pp.247–267.

1 Introduction: composites and crashworthiness

The combination of crashworthiness features implemented in the past few decades into racecar design has dramatically improved the safety of the racing practice and it has been observed that every component of the vehicle must be designed with an element of

crashworthiness built into it (see MIL-HDBK-17, 2006a). Previous research by Simula Technologies (2000) for NASA Langley has indicated that the four necessary conditions for survival are maintaining sufficient occupant space, providing adequate occupant restraint, employing energy-absorbing devices and allowing for a safe post-crash egress from the vehicle. A systems approach to aircraft or automotive crashworthiness means that the energy-absorbing components (e.g. nosecone), primary vehicle structure (e.g. the survival cell) and secondary systems (e.g. seats and restraint systems) must all be designed to work together to absorb the vehicle kinetic energy, thereby limiting the forces transferred to the occupants and slowing them to rest without injurious loading.

The introduction of composites in the primary structure of modern aircraft and ground vehicles presents special problems for the designer dealing with crashworthiness and the need to address these issues is witnessed by the creation of specific Working Groups, such as the Crashworthiness working group within the MIL-HDBK-17 handbook on composite materials. The brittle failure modes of many polymeric composite materials can make the design of energy-absorbing structures difficult. While metallic structures loaded in compression collapse by buckling and/or folding in an accordion-type fashion involving extensive local plastic deformation, composite structures fail through a combination of fracture mechanisms, involving fibre fracture, matrix cracking, fibre-matrix debonding and delamination damage, see Carruthers et al. (1998) and Hull (1991). Thus, the energy-absorbing behaviour of composites is not easily predicted, partly due to the complexity of these failure mechanisms and partly to the sensitivity of crash performance to manufacturing process variability, which can be significant in complex components. The overall response is highly dependent on a number of parameters, including the geometry of the structure, material system, crush speed and temperature. Thus, extensive substructure testing is usually required within a building block approach to the design of crashworthy structures, in order to verify that a proposed configuration will actually perform as intended, as suggested by the MIL-HDBK-17 (2006b). With composite materials, the engineer assigned to the task of designing for crashworthiness has the possibility of tailoring the response of the structure by operating on the fibre material and architecture, resin system, stacking sequence and relative combinations. Crash energy absorption with composite materials must come from innovative design, which compensates for their low strain to failure behaviour. Formula 1 (F1), see Savage et al. (2004), Savage (2006) and Bisagni et al. (2005), was the first racing league to make extensive use of Carbon Fibre Reinforced Polymer (CFRP) primary structures and currently the majority of premier racecar manufacturers, such as the Indy Racing League (IRL) discussed by Saccone (2003), the Championship Auto Racing Team (CART) by Swift Engineering Inc. (1999) and the Toyota Formula Atlantic, see Roberts et al. (2004) regularly employ composite structures. Since the late 1980s the Federation Internationale de l'Automobile (FIA) has introduced a series of regulations to ensure that racecars conform to stringent safety requirements and build quality, in the form of tests witnessed by Federation officials, in order to be granted race-worthiness certification. These criteria include a series of static loads applied to the chassis, which guarantee the strength and integrity of the survival cell and a series of requirements on the location and impact characteristics of the energy-absorbing devices. Each year the number and severity of these requirements increases in line with ongoing research and development in crashworthiness or in response to real-life accidents, see Savage et al. (2004) and Simula (2000). While F1 still constitutes the premier racing league, crashworthiness requirements for the other high-performance racing circuits

(e.g. Formula 3) are sometimes less stringent but mostly very similar in nature, as in the case of the Rear Impact (RIMP) test, originally introduced for F1 vehicles in 1997.

The Star Mazda Championship (Figure 1) series is a development series for open wheel racing in North America and is the largest 'spec' formula series in the USA. The fixed specification series, such as the Formula Atlantic per Roberts et al. (2004), require that pilots compete with equally matched vehicles, which differ only in the selection of suspension and aerodynamic settings. In order to provide additional safety for the drivers racing on an oval track, where the speeds are higher and the retaining walls are closer, a CFRP RIMP structure was developed. This paper summarises the design and development effort that led to the certification of the composite RIMP energy absorber, also referred to as rear crash attenuator, which consists of a thin-walled dispensable structure that greatly reduces the accelerations transmitted to the driver in the event of a rear collision (Figure 1).

Figure 1 Typical Star Mazda Championship racecar photographed after losing control on the oval racetrack and while spinning towards the wall. The CFRP RIMP is visible in the aft portion of the vehicle below the wing



2 Development of the RIMP

2.1 Design requirements

The RIMP was voluntarily introduced in the Star Mazda series for installation during the late part of the 2005 championship. Since at the time of development there was not a specific Star Mazda regulation, the certification procedure was carried on according to the requirements of the RIMP structure for the 2005 FIA Formula 3 Racing series, see FIA (2005, Articles 15.5.1 and 15.5.2 of Appendix J), of which the most relevant portion is briefly summarised here for completeness:

“An impact absorbing structure must be fitted behind the gearbox symmetrically about the car center line with its rearmost point between 550 mm and 620 mm behind the rear wheel center line. It must also have a minimum external cross section, in horizontal projection, of 9000 mm² at a point 50 mm forward of its rearmost point. This structure must pass an impact test and be constructed from materials, which will not be substantially affected by the temperatures it is likely to be subjected to during use. All parts which will be fitted behind the rear face of the engine and which could materially affect the outcome of the test must be fitted to the test structure. If suspension members are to be mounted on the structure they must be fitted for the test. The structure and the gearbox must be solidly fixed to the ground and a solid object, having a mass of 560 kg and traveling at a velocity of 10 m/s, will be projected into it. The object used for this test must be flat, measure 450 mm wide by 550 mm high and its lower edge must be at the same level as the car reference plane and must be so arranged to strike the structure vertically and to the car center line at 90 degrees. During the test, the striking object may not pivot in any axis and the crash structure may be supported in any way provided this does not increase the impact resistance of the parts being tested. The resistance of the test structure must be such that during the impact:

- Average deceleration of the object does not exceed 25 g,
- Maximum deceleration does not exceed 60 g for more than a cumulative 3 msec in the direction of impact,
- All structural damage must be contained within the area behind the rear wheel centerline”.

2.2 *Previous work*

From the numerous experimental studies that have been carried out on composite energy absorbing devices, it is generally accepted that thin-walled tubular structures offer the most weight-efficient solution. These tubular devices have been shown to absorb considerable amounts of impact energy as long as global (Euler) or local (wall) buckling is avoided, as summarised by Carruthers et al. (1998). The favourable failure modes are thus the ones that involve brittle fracture, in particular the splaying (or lamina bending) and the fragmentation (or transverse shearing) crushing modes, see Hull (1991) and Farley (1992). In the splaying crushing mode, crack growth is the predominant energy absorption mechanism, although bending and friction of the lamina bundles that form during the crush also contribute to dissipating energy. On the other hand, in the fragmentation crushing mode, the primary energy absorption mechanism is fracture of the lamina bundles, followed by inter and intralaminar cracking of the matrix. Unfortunately, there is no ‘thumb rule’ with which to predict the failure mode of a specific tube and the challenge for the engineer assigned to the design of these energy-absorbing structures is to identify and predict the appropriate geometric, material and loading conditions such that axial failure of the tubes is characterised by a progressive, stable collapse enabling high energy absorption. In general the design process of energy-absorbing devices needs to rely heavily upon an experimental database, but unfortunately there is a lack of standardised or otherwise commonly accepted practices for the characterisation of the energy absorbing characteristics of the composite structures or materials. A large part of the effort of the recently formed Crashworthiness Working Group of the MIL-HDBK-17 is directed to the development and standardisation, in conjunction with the ASTM D-30 Committee, of appropriate test methodologies for qualifying the energy absorption characteristics of composite systems.

Racecar manufacturers, see Savage et al. (2004) and Bisagni et al. (2005) have reported the use of circular specimens for the characterisation of the energy absorption of composite material systems for comparison purposes, while the Automotive Composites Consortium (ACC) Energy Management Working Group, under the supervision of the US Department of Energy (DOE), has made extensive use of square section tubes, see Browne (1998) and Browne and Johnson (2003). For non-circular tubes, the crushing behaviour is favourably influenced by well-rounded corners; the greater the corner radius, the higher the efficiency of energy absorption, see Savage et al. (2004). Rounded corners usually help to prevent flat segments from failing by local plate buckling, with associated plate strip buckling and much lower Specific Energy Absorption (SEA). The transition from lab-sized coupons to real structures is not seamless, as moving away from a simple tube to a more complex geometry tends to greatly reduce the energy-absorbing efficiency. For example, while a circular tube might exhibit a SEA of 80 kJ/kg, a more complex structure made from the same material, such as a side impact device, might exhibit a SEA of 60 kJ/kg, while in a component with high axial ratio, a nose box for example, the SEA can be further reduced to 35–40 kJ/kg. In general, it has been found that the highest amount of energy absorption is achieved by developing a sustained high-level crushing force, with little amplitude fluctuations. Furthermore, a general rule is that large initial peak forces should be avoided in order to limit the peak transmitted accelerations and to avoid unexpected concurrent failure modes to take place. This has been traditionally achieved by introducing a collapse ‘trigger’ mechanism into the structure, for example by chamfering one end or voluntarily reducing the local thickness of the laminate in a ‘weak spot’, see Thornton and Jeryan (1998).

It has been shown that hollow truncated cones can fail by progressive crushing with values of SEA sometimes exceeding those of axisymmetric tubes of the same material. However, the development of a stable crush front depends on the relationship between wall thickness, cross section diameter and semi-apical angle, which is not easily determined. In general, the SEA tends to decrease with increasing semi-apical angle and there appears to be a point of transition from stable to unstable collapse at angles between 15 and 20°. Contrary to what is commonly experienced with the failure of circular or square tubes, conical specimens do not require a collapse trigger mechanism to avoid initial catastrophic failure, but progressive crushing initiates automatically at the narrow end of the cone. This observation has proved very useful for the design and implementation of energy-absorbing devices in real life applications, due to the complexity of achieving the triggering mechanism, which results in noticeably increased manufacturing time and cost. Savage et al. (2004) suggest tapering of the geometry and of the lay-up within the confines of the envelope defined by the sport’s technical regulations in order to achieve the desired crush progression. Another important consideration in the selection of conical or otherwise tapered cross sectional members, is the ability to accommodate moderately off-axis loadings.

The RIMP is primarily an energy-absorbing component although, as in the case of the B.A.R.-Honda design in Savage et al. (2004), but it is also designed to transmit the rear wing and rear suspension loads to the chassis. It is also designed to withstand the jacking loads and support the rear light. The challenge is in finding a compromise between making the RIMP ‘soft’ for better crash performance, yet strong and stiff for sustaining the structural loads. However, the peak forces generated under impact are in the neighbourhood of 460 kN, while the resultant aerodynamic load is only 6.5 kN and the rear top wishbone load is around 18 kN. It is therefore the crash performance of the

RIMP that drives the design. The typical material selection and design procedure for the B.A.R.-Honda RIMP is reported by Savage et al. (2004) and Savage (2006) and it involves a simple energy balance, whereby the minimum crush distance is calculated. The laminate thickness and lay-up is sized based upon the SEA measured in the quasi-static and drop-tower impact crushing of circular tubes. The surface area of the cross section is measured from CAD drawings at discrete intervals (25 mm), the predicted energy absorption is calculated and a factor is added to account for structural inefficiencies. Although there are explicit, non-linear finite element codes suitable for the dynamic modelling of crash events, the complexity of the failure mechanisms of fibrous composites is such that the RIMP is developed mainly experimentally.

2.3 Material selection

When choosing the material from which the energy-absorbing device will be made, the toughest resin systems become particularly appealing. However, rubber-modified epoxies have a lower operating temperature range and some of the impact structures may require a degree of heat resistance, as highlighted by Savage et al. (2004). Such is the case for the rear attenuator, which is situated right behind the engine, hence necessitating the use of a more brittle, higher temperature epoxy matrix.

The energy absorption characteristics of some typical Advanced Composites Group motor-sport composite material prepreg systems were previously characterised by dynamic testing of thin-walled tubular members, see Masini and Feraboli (2002). The range of fibres investigated spanned between commercial-grade and high-modulus, while the resins belonged to a similar family of commercial-grade epoxies and the results are reported in Table 1. The fibre architecture common to all systems investigated was a 2×2 twill fabric, oriented axially (0/90 direction). While unidirectional material can be more efficient in energy absorption, fabric reinforced materials are often preferred in impact structures because of their in-plane symmetry which favours the onset of a stable crush. Disagreement has been found in the literature between the energy absorption efficiency of fabric and tape materials. Some researchers report the unidirectional tape material to be more efficient, see Farley (1992), while others report mixed results, see Bisagni et al. (2005).

Table 1 SEA (kJ/kg) of typical motor-sport material systems from Masini and Feraboli (2002). Different fibre and resin materials are shown for the same fabric architecture.

<i>Fibre/resin</i>	<i>MTM-49</i>	<i>MTM-249</i>	<i>MTM-28</i>	<i>MTM-228</i>
T300	45	–	–	–
T800	47	42–50	56	53
IM7	–	53	–	58
T1000	–	44	–	52

The testing by Masini and Feraboli (2002) was performed on square conical specimens, with a slight taper and open at the two ends. The cones were tested at room temperature in a drop tower at an impact velocity of 6 m/s, using a crosshead weighing approximately

200 kg. Savage (2006) summarised the effects of various mechanical properties such as tensile strength and modulus, as well as interlaminar shear strength and Mode I Fracture Toughness on the SEA characteristics of two Cytec material systems used by the B.A.R. F1 team. From those results it is possible to observe that the SEA increased for increasing values of strength and toughness, and decreasing values of the principal Young's modulus and similar trends can be qualitatively seen in Table 1 for the present investigation. Although the data is limited and it cannot be used as a general rule, it is a common rule of thumb that can be used in the preliminary design stages. The material chosen is T300/MTM49, having 42% resin content and a 250 F degree-cure, toughened system. When choosing the material from which the device will be made, one should aim to use intermediate modulus fibres and the toughest resin systems.

2.4 Dimensioning of the cone

Preliminary sizing of the RIMP is performed considering that the kinetic energy at impact is:

$$E = \frac{1}{2}mV^2 = 30.7 \text{ kJ} \quad (1)$$

where m is the vehicle mass (614 kg) and V the impact velocity of 10 m/sec. The average impact force, corresponding to the maximum allowable deceleration rate of 25 g is given by:

$$F = ma = mgG = 150.5 \text{ kN} \quad (2)$$

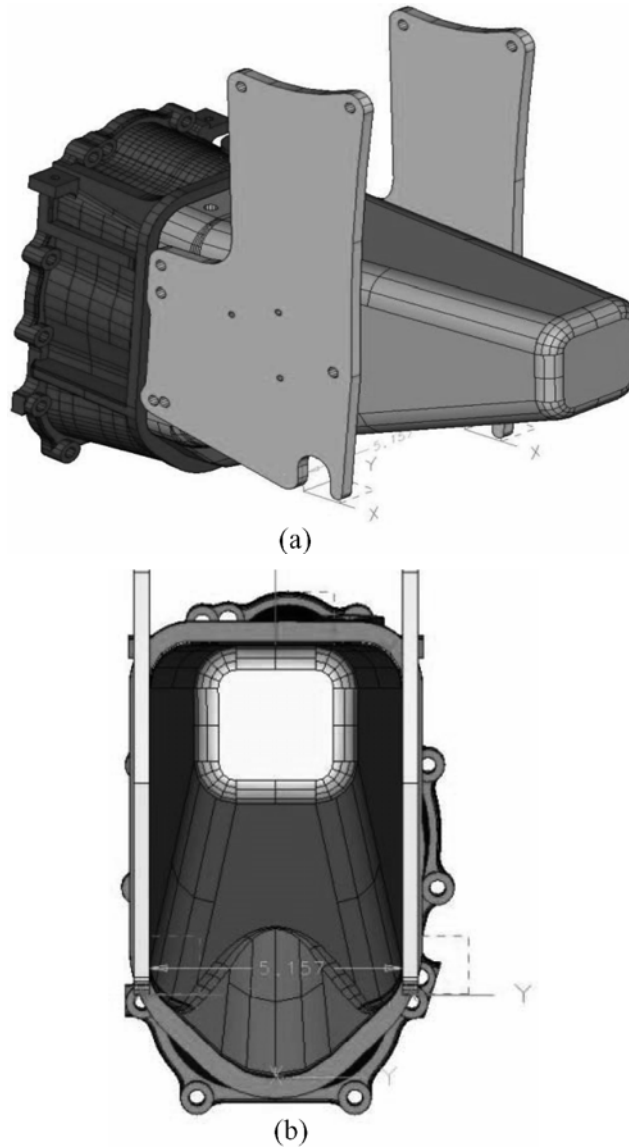
where g is the number of g 's and G is the acceleration due to gravity. With a simple energy balance, equating the work done by crushing the box to the available kinetic energy and solving for the axial displacement D :

$$D = \frac{E}{F} = \frac{30.7}{150.5} \quad (3)$$

It is possible to obtain a preliminary estimate of the box length. The assumption is that the system absorbs, constantly from the beginning of the crush and through the duration of the event, the entire amount of energy available, which is obviously a rough and non-conservative estimate. A similar sizing procedure was briefly mentioned by Savage et al. (2004). A length of 204 mm is therefore the minimum required to dissipate the maximum amount of kinetic energy. Using more conservative values of 20 and 15 g for the average crush force, absorber lengths of 255 and 340 mm, respectively, are required to dissipate the same amount of energy. Due to aerodynamic constraints, the maximum available length of the tail cone is 343 mm, while maximum wall thickness is 3 mm. This value is dictated by the maximum gap allowed at the root of the cone, in the region where it is mechanically fastened between the wing supports and the gearbox housing.

The final RIMP geometry, resulting from having to fit within the existing envelope, is essentially a truncated pyramid, having the minor base nearly perpendicular to the major base (Figure 2(a) and (b)). The minor base has a square cross section of dimensions 81.3 mm \times 81.3 mm, while the major base is roughly rectangular in shape and has dimensions of 130.8 mm \times 209.6 mm.

Figure 2 Three-quarter (a) and frontal (b) views of the solid model of the RIMP, also showing the gearbox cover and the wing supports



2.5 Competing cone designs and manufacturing solutions

Two cone designs are manufactured and experimentally characterised. While the overall geometry is the same, as is the fibre/resin system, the two designs come from opposite philosophies. One design (FQI) favours a quasi-isotropic lay-up, with axial, angle and hoop plies, while the other (K0/45) has a greater content of angle plies but no fibres in the hoop direction. The two laminate lay-ups are noticeably different, as are the resulting macroscopic laminate properties.

Both design incorporate a trigger mechanism, which is a built-in imperfection that favours the initiation of the crush at the desired end and a stable progression. Although not required in the case of a conical or pyramidal section, it is incorporated for added safety. Both fabric and tape prepregs are used and they have a nominal thickness of 0.25 mm and 0.125 mm, respectively.

A first cone, denoted K0/45, is designed to have a somewhat balanced degree of 0 and $\pm 45^\circ$ fibres. The wall thickness of the laminate is constant through the cone at 2.8 mm and the modulus in the axial (longitudinal) direction is much greater than in the 'circumferential' direction. About 54% of the fibres are unidirectional tape plies oriented in the [0] direction, while the remaining plies are ± 45 fabrics that provide a noticeable degree of shear stiffness. In the initial trigger zone of 38.1 mm in length, the thickness is 2.0 mm and the UD [0] ply content is reduced to 35%, thus giving a 'softer' laminate. While the absence of [90°] plies produces very low E_y , it has been shown by Farley (1992) that ply orientation has little influence on the SEA for angles exceeding 45° . The K0/45 cone is designed to be conservative, because of the thicker lay-up and heavier construction and easy to manufacture thanks to its simple stacking sequence. Its laminate properties are summarised in Table 2.

Table 2 Dimensions and elastic properties of the equivalent laminate for the various segments of the two tail cone designs

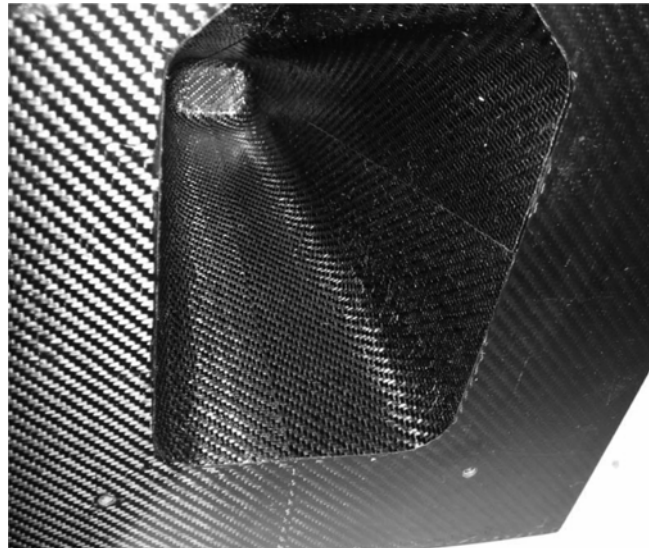
	<i>K0/45</i> <i>Section 1</i>	<i>K0/45</i> <i>Section 2</i>	<i>FQI</i> <i>Section 1</i>	<i>FQI</i> <i>Section 2</i>	<i>FQI</i> <i>Section 3</i>
Thickness mm	2.0	2.8	1.5	2.3	3.0
Length mm	38.1	304.8	76.2	165.1	101.6
E_x GPa	44.4	58.9	48.2	51.6	53.8
E_y GPa	17.8	16.3	48.3	41.9	38.7
G_{xy} GPa	17.0	13.3	7.0	8.3	8.4
ν_{xy}	0.711	0.659	0.121	0.167	0.195

A second cone, denoted FQI, employs a more complex stacking sequence and ply schedule and is designed for improved energy absorption because of its more complex ply schedule. The advanced design employs a well-balanced (fibres in the axial, angle and hoop directions) and homogenous ply schedule (plies of same orientation are not grouped together), which alternates layers of tape and fabric stacked at different angles through the thickness. The cone also features a three-stage design, comprised of three sections of progressively increasing laminate thickness. Its design features a nearly quasi-isotropic lay-up, particularly in the initiation region, which comprises the first 76.2 mm. The lay-up of the initial segment, which is 1.5 mm thick, is: $[(0/90)/90/(0/90)/0_2/(0/90)/(\pm 45)/90]_T$. The lay-up becomes progressively 'harder' and the second and third stages see the introduction of more [0] tape and $[\pm 45]$ fabric and an increased thickness of 2.3 mm and 3.0 mm, respectively. According to Hull (1991), using a [0]:[90] ply ratio of 3:1 or 2:1 yields the most desirable results in terms of SEA. At the same time, inclusion of the [0] plies within the [90] plies at the inner and outer diameters yields far greater SEA capabilities than grouping all [0] plies on the inside or

the outside or interleaving them through the thickness. The details of the ply schedule and elastic properties of the equivalent laminates for the three stages are also reported in Table 2.

The prepreg sheets are cut into patterns, each having the shape of one of pyramid's faces. Every ply is slightly wider than the actual dimension of the face and the excess material is wrapped around the corner onto the neighbouring face. Overlapping the plies on the faces rather than at the radii prevents material build-up, hence prevents the corners from behaving as hard points during a crash event. The mould (Figure 3) is manufactured with special tooling carbon/epoxy prepreg, see Feraboli and Masini (2004). The choice of using a female (internal) tool is mainly given by aesthetic considerations, which require the fabric weave to have a good surface finish on the outside.

Figure 3 RIMP moulding tool, also made of CFRP. The female tool was chosen due to aesthetic considerations

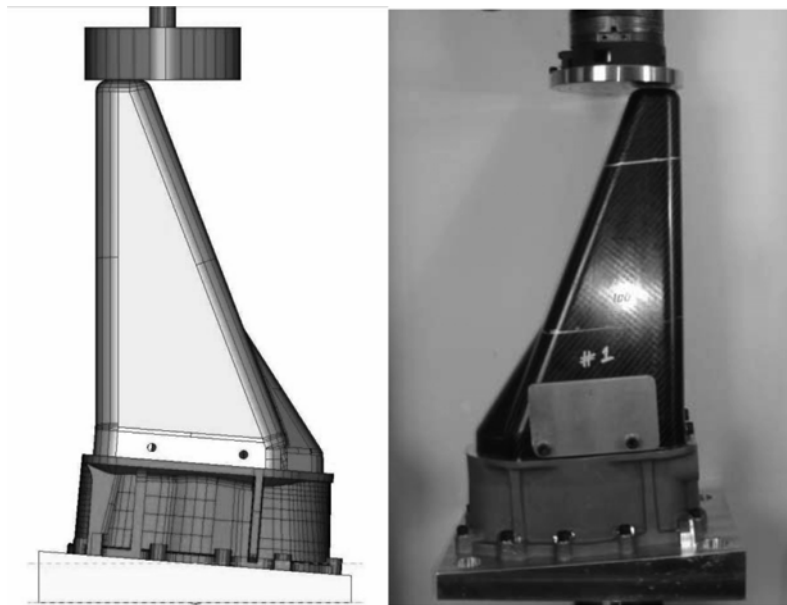


2.6 *Quasi-static and dynamic test setups*

The two competing tail cone designs are tested in quasi-static axial compression in a 222.4 kN hydraulic mechanical test frame under load control. Unfortunately, due to the laboratory's test machine stroke limitations, only a portion (slightly over 180 mm) of the total length (343 mm) of the cone are tested. Since the RIMP/ gearbox assembly is at an angle of 4.5° from the perpendicular to the car centreline, a special fixture (Figure 4) is developed to secure the assembly to the test frame. This fixture consists in an aluminium plate of variable thickness, which is fastened by means of a single 25.4 mm hexagonal head bolt to the base of the test machine. The bolt location is selected to be coaxial with the centre of gravity of the truncated cone and of the machine's crosshead. The fixture is designed to ensure that the crosshead contacts the outermost side of the truncated cone at a square angle with the car centreline and that mostly axial loading occurs during the majority of the stroke. This scenario closely reproduces the test conditions contained in

the FIA Formula 3 crash test specification (2005) and is representative of the actual scenario of a vehicle crashing backwards into a barrier during a race. The cone is fastened onto the gearbox casing by means of six screws, which pass through the composite laminate in appositely machined holes. These screws need to carry both normal and shearing forces due to the oblique nature of the fixture. Two aluminium platelets are installed on each side to simulate the presence of the rear wing supports. The gearbox casing is fastened to the aluminium fixture by means of 12 screws of smaller diameter, partly visible in Figures 2(a), (b) and 4. The RIMP/gearbox/fixture assembly is shown in Figure 4 with the upper moving plate in the test frame. The load cell measures the load, while the stroke is known by assigning the crosshead speed at the beginning of the test, which in this case is 12.7 mm per minute.

Figure 4 Solid model and actual geometry of the setup for quasi-static crushing of the RIMP



The impact tests are performed at the Exponent facility near Phoenix, AZ. The longitudinal velocity is selected to be 10.0 m/s and is measured using a speed trap located closely to the point of impact to account for frictional losses of the sled along the rails. The severity of the event is measured with two longitudinal accelerometers and is reported in g 's according to common practice, see Savage et al. (2004). The force is then calculated knowing the mass of the sled. The accelerometers are mounted on the moving sled and the data is filtered using a SAE J211 class 60, 100 Hz filter. Velocity and stroke are calculated by integrating the acceleration data. One off-board real-time video camera and one off-board high-speed video camera are used to record the event.

The rear crash attenuator/transmission gearbox assembly is secured to the aluminium fixture used in the laboratory tests to compensate for the obliquity of the RIMP/gearbox assembly. The mounting angle of the cone is approximately 0.3° nose down from horizontal. The rear wing assembly, comprised of the supporting plates and of the two-tier wings, is installed on the RIMP assembly to simulate the standard race-ready

configuration. The entire assembly is then attached to a fixed-barrier and impacted by a sled consisting of a flat steel plate, having dimensions 450 mm × 550 mm mounted on a larger sub-barrier (Figure 5). The test configuration, test procedure and data reduction is performed in accordance with the requirements of the International Sporting Code, FIA, Appendix J, Article 275, 2005 Formula 3 Technical Regulations, Paragraph 15.5.2, see Bisagni et al. (2005).

Figure 5 Crash test setup showing the RIMP/gearbox/wing assembly and the impacting plate mounted on the moving sled



3 Results and discussion

3.1 *Quasi-static test results*

The Load-Stroke diagrams for the two cones are shown in Figure 6, which shows an initial nearly elastic portion, up to 12.7 mm of displacement. For the K0/45 cone, the wall thickness increases from 2.0 to 2.8 mm after 38.1 mm, where a second linear portion terminates. Progressive crushing then begins, with serrated oscillations around a mean value, which increases with a very low slope, due to the progressive increase in cross-section. In the case of the FQI cone, the laminate is crushed at fairly low but constant load levels until the thickness increases from 1.5 mm to 2.3 mm, then it jumps at a larger crushing load level, which is also nearly constant. Towards the end of the available stroke, an inexplicable drop in the average load is observed and further work needs to be performed to determine its cause. In general, the greater thickness of the cone K0/45 yields higher average loads, as given in Table 3.9

Figure 6 Quasi-static load-stroke diagrams for the two tail cones

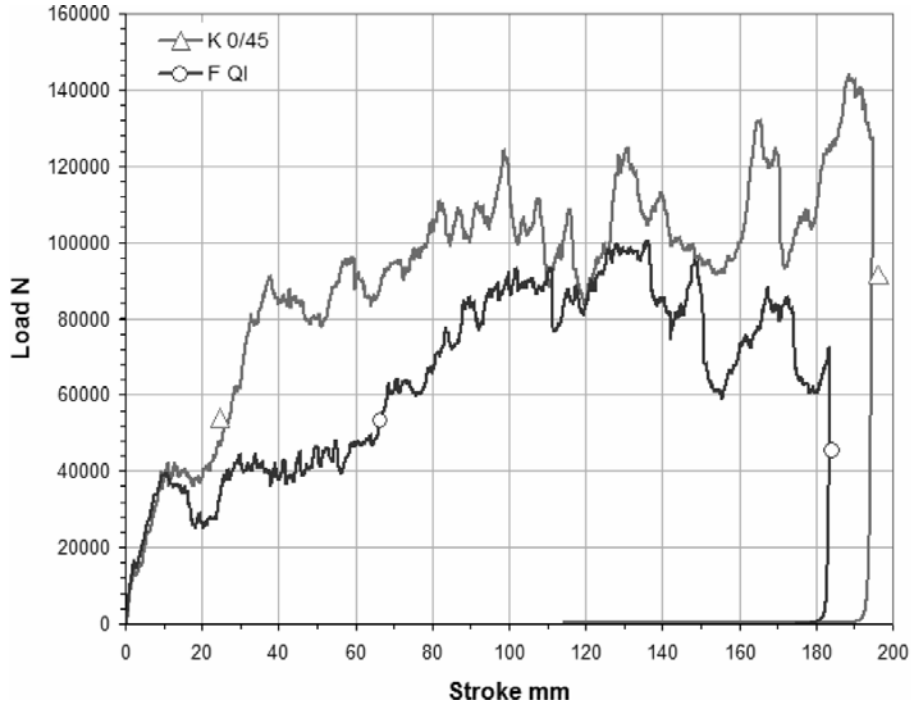


Table 3 Static and dynamic results for the three tail cones tested

	<i>Initial weight kg</i>	<i>Peak force kN</i>	<i>Avg. force kN</i>	<i>Total stroke mm</i>	<i>EA kJ</i>	<i>SEA kJ/kg</i>	<i>Avg. stress MPa</i>
K0/45	0.850	144.35	93.52	195.1	17.9	49	67.3
FQI	0.737	100.55	64.90	183.9	11.8	41	66.5
DYN K0/45	0.862	197.04	90.87	341.4	30.8	33	–

Conventionally, the average crush force is calculated as follows:

$$F_{avg} = \frac{EA}{l} \tag{4}$$

where EA is the total energy absorbed and *l* is the total crush length.

Both specimens clearly show a progressive and stable failure, with initial collapse forces that are lower or equal than the subsequent crush forces for the same laminate thickness. The failure progression for specimen K0/45 and FQI are shown in Figures 7 and 8, respectively. Both cones are characterised by a fragmentation/transverse shearing failure mode, which is very desirable for its elevated energy-absorbing capabilities. However, they exhibit large fronds of semi-intact material, particularly in the case of the K0/45 cone, where a larger, longer frond is bent outward (Figure 7). The FQI cone is instead characterised by more uniform, equally sized frond on all three vertical walls, while the oblique wall is also bent toward the inside of the cone (Figure 8).

Figure 7 Crush progression and failure of the K0/45 cone

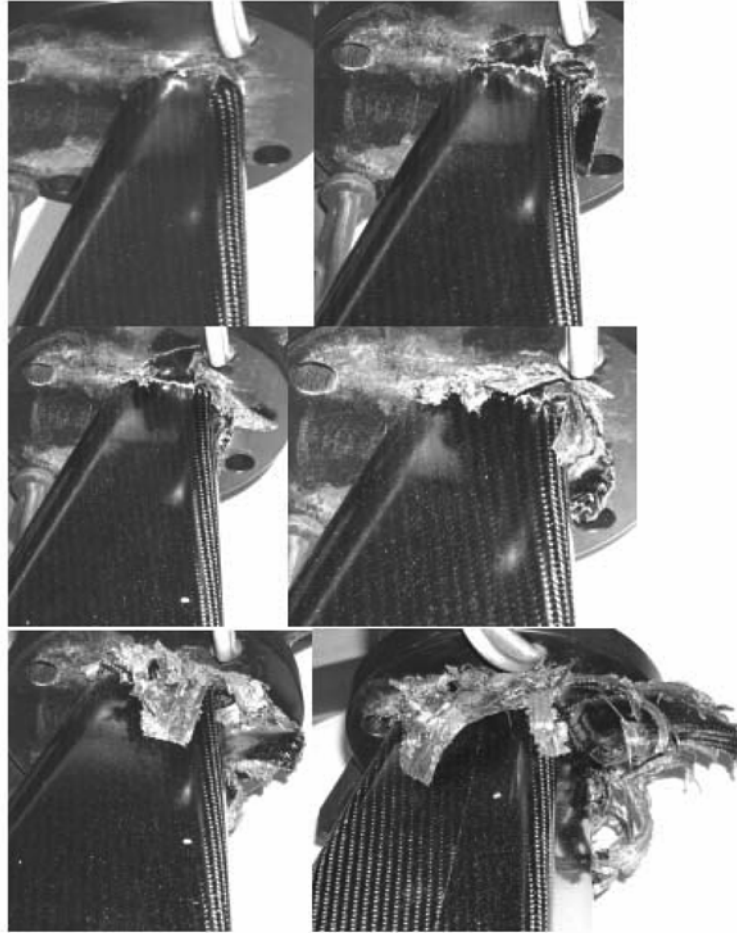
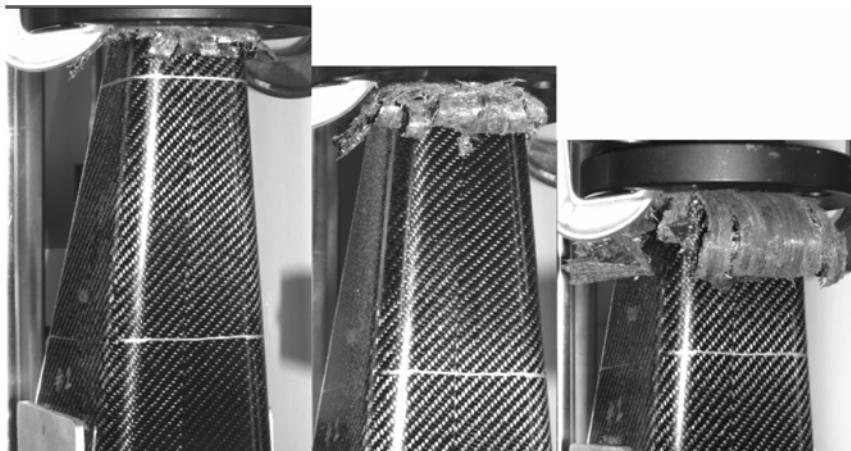


Figure 8 Crush progression and failure of the FQI cone



The total EA during the crushing is shown with respect to stroke in Figure 6 for the two tubes. For variable cross-section tubes, the SEA is given by:

$$SEA = \frac{EA}{\rho A_i l} \quad (5)$$

where EA is the total EA at the end of the crush, ρ is the density, A_i is the cross sectional area at a generic section i and l the total crush length. With values of SEA of 49 and 41 kJ/kg for the K0/45 and the FQI cones, respectively, very good agreement can be observed between the theoretical (thin lines) and the measured (thick lines) curves in Figure 9. The predictions are based on results from previous unpublished work by Masini and Feraboli (2002), which had indicated SEA values of 45 kJ/kg for the present system, Table 1. The jump in the predicted curves is due to the abrupt change in thickness at the transition from stage 1 to stage 2 of cone FQI. The relationship between absorbed energy and stroke is then roughly:

$$EA = SEA \rho A l \quad (6)$$

From the Load-Stroke diagram, the average crushing stress can be calculated alternatively using:

$$\sigma(x) = \frac{P}{(2h \tan \theta + 2t(x) + D_i)^2 - (2h \tan \theta + D_i)^2} \quad (7)$$

where P is the instantaneous value of the load, h is the stroke, theta is the semi-apical angle, t is the wall thickness (which is here indicated as a function of x for non-uniform wall thickness) and D_i is the internal diameter. The above equation is valid for any truncated cone. However, in the majority of cases, energy absorbers are thin-walled structures and simplified formulas can be used. Since the square cross-section is 21.5% ($1-\pi/4$) more than the area of the enclosed circle, it is possible to obtain:

$$\sigma(x) = \frac{\pi}{4} \frac{P}{\pi D(x) t} = \frac{P}{4t(2h \tan \theta + 2t(x) + D_i)} \quad (8)$$

where $D(x)$ is the mean diameter of the thin-walled tube, accounting for the possibility of non-uniform wall thickness through the length of the cone. The two equations have given results within 2% of each other for the present geometry. A plot of the crushing stress against the stroke for the two cones is shown in Figure 10 and the results are given in Table 3. It can be seen that the average crushing stress for the two cones is nearly identical, with only an initial difference where the FQI cone appears to achieve the sustained crushing stress much earlier than the K0/45, hence it may be argued whether the crushing stress is a useful tool to compare crush responses.

3.2 Crash test results

Because of the slightly higher energy absorbing characteristics of the K0/45 solution and because of its manufacturing simplicity, a decision is made to move forward with such design for the certification via dynamic test. The added complexity of the FQI lay-up does not appear to improve the energy-absorption characteristics of the structure.

Figure 9 Plot of the measured and theoretical absorbed energy curve during the quasi-static crushing of the two tail cones

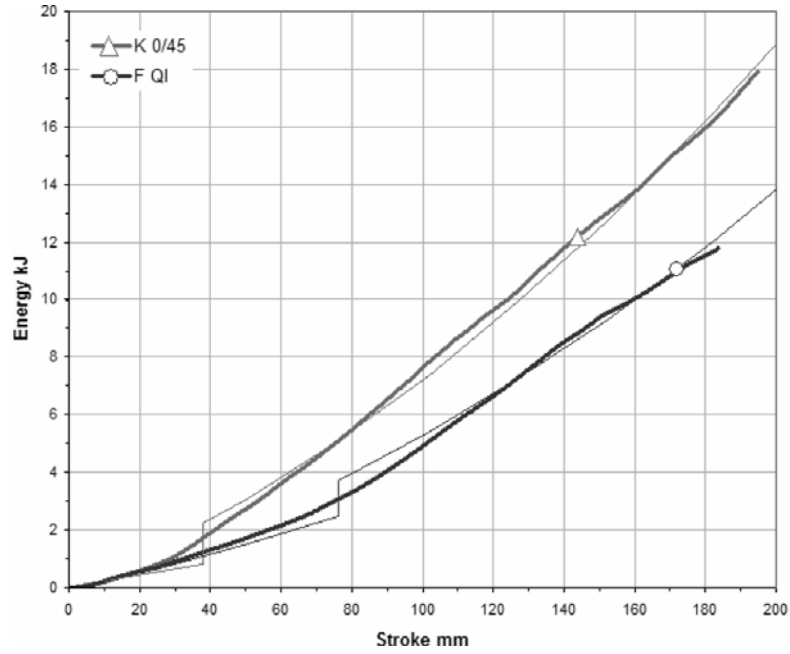
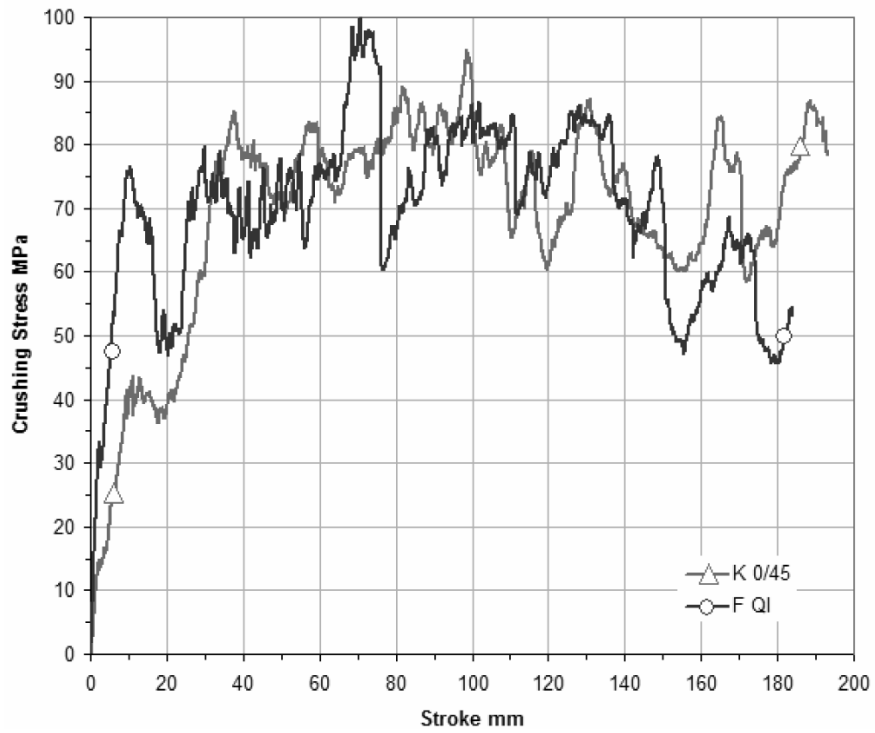


Figure 10 Plot of the crushing stress during the quasi-static crushing of the two tail cones



The average deceleration rate is 15.5 g and it is calculated between the time interval in which the impacting surface first contacts the test item until sled direction reversal occurs. The entire event lasts 70 ms, with the cone crushing the entire length of 343 mm. The reported maximum deceleration sustained for 3 ms is 28.8 g and it is defined as the value in which the deceleration level is sustained at equal or greater magnitude for a cumulative time of 3 ms. The absolute maximum acceleration measured in the test is 32.71 g. The results for force, velocity and stroke progression are plotted in Figure 11. Unlike the laboratory test, which was halted shortly after 178 mm of crush, the dynamic test has enough energy to crush the entire cone. The two large spikes visible in the acceleration trace are due to the first contact of the sled with the wing support plates and the wing itself and the subsequent contact with the metallic gearbox after the entire cone has been disintegrated. The event is recorded from high-speed cameras and stills are extracted at intermediate points during the impact. From the pictures of the specimen taken after the dynamic axial collapse (Figure 12), it can be seen that similar splaying fracture mechanisms occur as in the quasi-static crush test. However, the specimen exhibits larger (more pristine) fronds, indicative of somewhat lower energy absorption. Furthermore, there appears to be a visible interlaminar separation between some of the tape and fabric plies, whereby the outer plies bent outward while the more inner plies crushed or bent inward. This phenomenon was not visible in the quasi-static crush test where the fronds bent uniformly outward. Lastly, a large intact portion of the RIMP corresponding to the lower, inclined face detached before being crushed and was found in pristine conditions. The results for the dynamic test are also given in Table 3.

Figure 11 Acceleration, velocity and stroke progression during the impact event

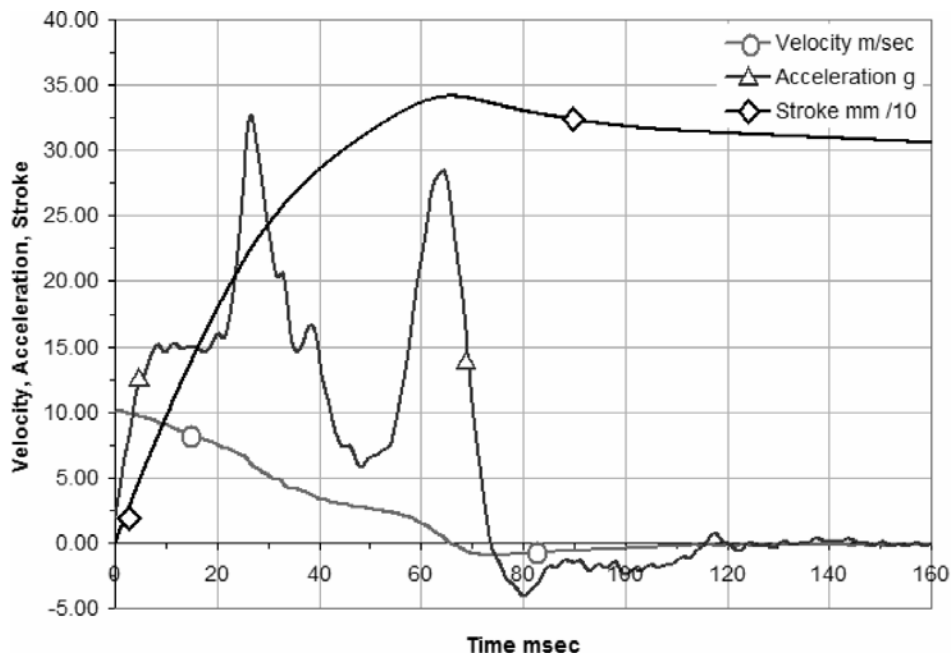
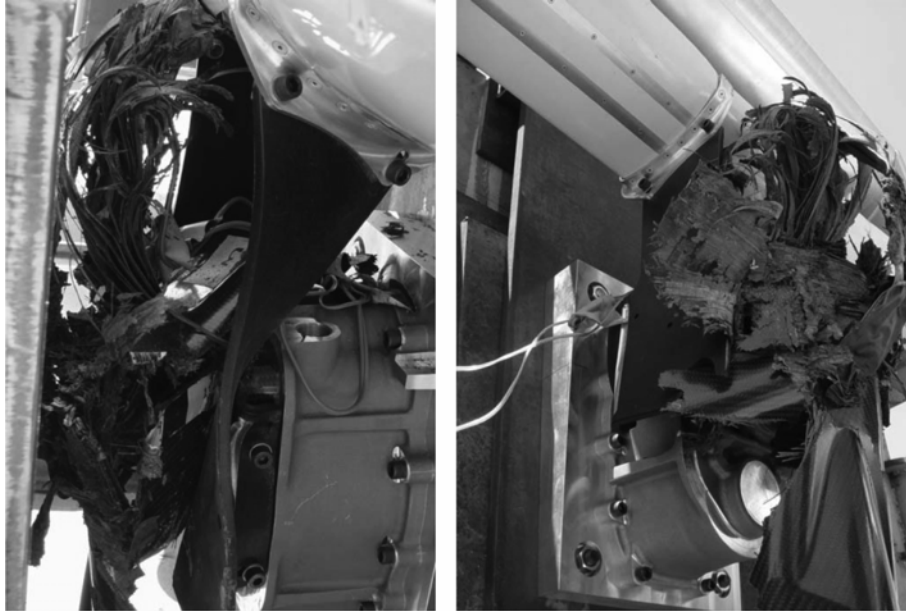


Figure 12 Specimen after dynamic test shows fracturing behaviour similar but not identical to the quasi-static specimen



3.3 Discussion

It has been previously shown by Browne and Johnson (2003) that quasi-static crush tests can lead to over-optimistic assumptions with regards to SEA values, which in turn can lead to unconservative and unsafe designs. A comparison between quasi-static and dynamic results on the K0/45 cone appears to confirm those observations, as shown in Figures 13 and 14 and in Table 3. The dynamic Load-Stroke diagram does not exhibit the serrated oscillations visible in the quasi-static curve, partly due to the limits in data acquisition rate and partly to the use of a filter to suppress undesired fluctuations present in dynamic data. The average crush force values for the quasi-static and the impact tests, given in Table 3, are very close if the latter is calculated by means of Equation 4 over the entire crush length. However, Figure 13 shows a noticeably higher average force for the quasi-static test (93.52 kN versus 77.68 kN) in the first 190 mm of stroke. Similarly, the EA up to that point of stroke is higher for the quasi-static test (17.8 kJ versus 14.8 kJ), as shown in Figure 14 and the SEA for that portion of the crush is then 42 kJ/kg, which is still noticeably lower than the quasi-static test, but not as much as from Table 3. So there is at least a 15% difference in crush force and SEA between the quasi-static and dynamic results, which is consistent with other findings by Browne and Johnson (2003).

In general, this difference can be attributed to three factors, namely the filtering of the signal (which reduces the accuracy of the data for integration), a possible strain-rate dependence of the coefficient of friction and a different friction coefficient for the crushing surfaces used in the two tests. Previous research by Hull (1991) and Farley (1992) has shown that a great deal of energy absorption (30–50% of the total), particularly when large fronds are created, is dissipated in friction between the fronds and the crushing surface. Therefore, if the surface of the impacting sled plate is smoother

than the laboratory-crushing surface or otherwise facilitates the sliding of the fronds, lower energy absorption will be measured. Future work will ensure that the exact same surface finish is used for the crushing surfaces in the laboratory and in the crash test setup.

Figure 13 The quasi-static and impact load-stroke diagrams show the little influence of test speed in crushing response

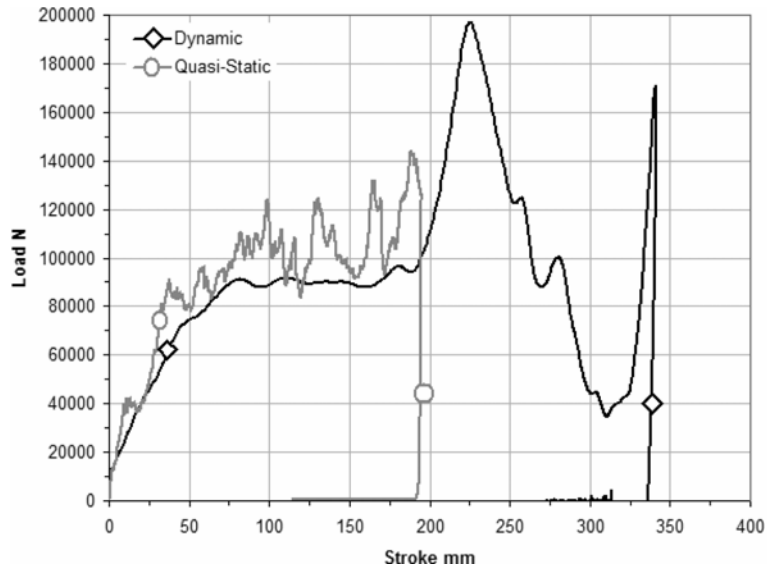
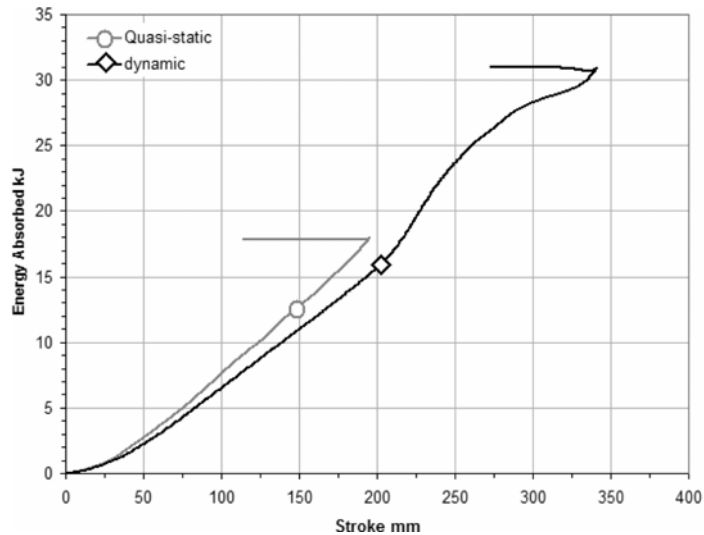


Figure 14 The diagram shows the similarity between the quasi-static and impact energy absorption



A last consideration that needs to be made is that only one test per cone configuration was performed due to budget and time constraints, therefore it was not possible to assess the potential variability associated with the test. Such variability could result from both

test setup and manufacturing imperfections, hence it could greatly reduce (or increase) the amount of difference between the quasi-static and the dynamic results.

Although very useful to gain understanding in the crush response of the cone designs, quasi-static tests need to be used with care when results from laboratory experiments are transferred to sled impact scenarios. Also, for future research it would be more useful to perform drop-tower impact tests on laboratory specimens at somewhat similar impact velocities rather than employing a purely quasi-static setup.

With regard to lay-up and laminate design, it appears that, although a dynamic test on the FQI as well as repetitions for each of the two designs would be necessary to really compare them adequately, the K0/45 performed better than the more complex FQI. It appears therefore that the macroscopic elastic properties of the equivalent laminate play a larger role than the specific ply schedule within the laminate. The difference in the results from two cones tested in a quasi-static fashion appears to be mostly attributable to the difference in 'circumferential' modulus (E_y) versus shear modulus (G_{xy}) for the two laminates, which exhibited very similar axial moduli (E_x). Also, for the very limited amount of weight saved between the FQI and the K0/45, the reduced wall thickness does not make up for the decreased SEA of the cone. However, although the simpler K0/45 RIMP performed better than the FQI one, it is not possible to explore the full extent of the latter, more advanced design. In fact, the laminate thickness is designed to increase noticeably in the third stage and had the quasi-static test not been interrupted prematurely, the cone could have led to more performing results. In general, for future improvements, the FQI lay-up could be revisited and the first stage could be reduced in length to the same extent as the K0/45 one and increased in thickness to the same level as the second stage. The second and only other stage would then be increased to the maximum allowed thickness of 3 mm for the entire remaining length of the cone.

4 Conclusions

Development of the thin-wall CFRP RIMP attenuator for the Star Mazda Championship racecar series was discussed in detail. Although large margin for improvement is still present, the preliminary design of the RIMP has passed the crash test certification based on the international motor-sport specifications for Formula 3. Quasi-static crush testing has shown to lead to greatly unconservative estimates of the SEA characteristics of the RIMP, although fairly good agreement between quasi-static and dynamic tests was observed in terms of overall load-stroke response and failure behaviour. From the study it appears that wall thickness and shear modulus have greater influence than ply schedule and circumferential modulus on the energy absorption capabilities of the structure.

Acknowledgements

The authors would like to thank Gary Rodriguez (Star Mazda Racing), Paul Kuhl, Kirk Fields and Andy Galloway for their suggestions and technical contributions in the development of the RIMP. Swift Engineering would also like to thank the American Society for Composites (ASC) for having bestowed on them the 2004 Best Paper Award for their presentation within the special session on High Performance Composites for

High Performance Cars (HPC4HPC). The authors would lastly like to thank the two anonymous referees for having performed a very thorough review, which greatly improved the quality of this paper.

References

- Bisagni, C., Di Pietro, G., Fraschini, L. and Terletti, D. (2005) 'Progressive crushing of fiber-reinforced composite structural components of a Formula 1 racing car', *Composite Structures*, Vol. 68, No. 4, pp.491–503.
- Browne, A.L. (1998) 'Automotive composites consortium generic tube crush program: dynamic crush tests of resin transfer molded tubes', *Proceedings of the 13th ASC Annual Technical Conference*, September, Baltimore, Maryland.
- Browne, A.L. and Johnson, N.L. (2003) 'Dynamic axial crush of automotive rail-sized composite tubes Part 5: effects of test conditions including impact velocity and temperature', *Proceedings of the 18th ASC Annual Technical Conference*, September, Gainesville, FL.
- Carruthers, J.J., Kettle, A.P. and Robinson, A.M. (1998) 'Energy absorption capability and crashworthiness of composite material structures: a review', *Applied Mechanics Reviews*, Vol. 51, pp.635–649.
- Farley, G.L. (1992) 'Relationship between mechanical-property and energy-absorption trends for composite tubes', *NASA TP 3284, ARL-TR-29*, December.
- Feraboli, P. and Masini, A. (2004) 'Development of carbon/epoxy structural components for a high performance vehicle', *Composites Part B*, Vol. 35, No. 4, pp.323–330.
- FIA (2005) 'Art 15.5: safety structures', *Formula 3 Technical Regulations, Appendix J*, Article 275, p.19.
- Hull, D. (1991) 'A unified approach to progressive crushing of fibre-reinforce composite tubes', *Composites Science and Technology*, Vol. 40, pp.377–421.
- Masini, A. and Feraboli, P. (2005) 'ACG material systems for energy absorption', *Internal Communication, Automobili Lamborghini*, May.
- MIL-HDBK-17 (2006a) 'Crashworthiness and energy management', *Rev. G.*, Vol. 3, Ch. 14, Available at: www.mil17.org.
- MIL-HDBK-17 (2006b) 'Building block approach for composite structures', *Rev. G.*, Vol. 3, Ch. 4, Available at: www.mil17.org.
- Roberts, N., Huschilt, T., McLarty, D. and Norris, C. (2004) 'Composite design and manufacture of the swift Toyota Atlantic race car', *High Performance Composites for High Performance Cars (HPC4HPC)*, *Proceedings of the 19th ASC/ASTM Joint Annual Technical Conference*, October, Atlanta, Georgia.
- Saccone, M. (2003) 'Composite design procedures for racing cars at Dallara Automobili', *Proceedings of the Third SPE Automotive Composites Conference and Exhibition*, September, Detroit, MI.
- Savage, G. (2006) 'Enhancing the exploitation and efficiency of fibre-reinforced composite structures by improvement of interlaminar fracture toughness', *Engineering Failure Analysis*, Vol. 13, pp.198–209.
- Savage, G., Bomphray, I. and Oxley, M. (2004) 'Exploiting the fracture properties of carbon fibre composites to design lightweight energy absorbing structures', *Engineering Failure Analysis*, Vol. 11, No. 5, pp.677–694.
- Simula Technologies (2000) 'A systems approach to general aviation occupant protection', *NASA Langley Research Center Final Report*, TR-00046, June.
- Swift Engineering Inc. (1999) 'Aero testing enables race car designers to hone racer's edge', *High Performance Composites*, March/April, Ray Publishing, pp.64–66.
- Thornton, P.H. and Jeryan, R.A. (1998) 'Crash energy management in composite automotive structures', *International Journal of Impact Engineering*, Vol. 7, No. 2, pp.167–180.